# Origin of magnetic excitation gap in double perovskite $Sr_2FeOsO_6$

A. E. Taylor,[1] R. Morrow,[2,3] M. D. Lumsden,[1] S. Calder,[1] M. H. Upton,[4] A. I. Kolesnikov,[1] M. B. Stone,[1] R. S. Fishman,[5] A. Paramekanti,[6,7] P. M. Woodward,[2] and A. D. Christianson[5,1,*]

[1]*Neutron Scattering Division, Oak Ridge National Laboratory, Oak Ridge, Tennessee 37831, USA*
[2]*Department of Chemistry, The Ohio State University, Columbus, Ohio 43210-1185, USA*
[3]*Leibniz Institute for Solid State and Materials Research Dresden IFW, Dresden D-01069, Germany*
[4]*Advanced Photon Source, Argonne National Laboratory, Argonne, Illinois 60439, USA*
[5]*Materials Science and Technology Division, Oak Ridge National Laboratory, Oak Ridge, Tennessee 37831, USA*
[6]*Department of Physics, University of Toronto, Toronto, Ontario, Canada M5S 1A7*
[7]*Canadian Institute for Advanced Research, Toronto, Ontario, Canada M5G 1Z8*

(Received 1 May 2018; revised manuscript received 15 August 2018; published 12 December 2018)

$Sr_2FeOsO_6$ is an insulating double perovskite compound which undergoes antiferromagnetic transitions at 140 ($T_{N1}$) and 67 K ($T_{N2}$). To study the underlying electronic and magnetic interactions giving rise to this behavior we have performed inelastic neutron scattering (INS) and resonant inelastic x-ray scattering (RIXS) experiments on polycrystalline samples of $Sr_2FeOsO_6$. The INS data reveal that the spectrum of spin excitations remains ungapped below $T_{N1}$, however below $T_{N2}$ a gap of 6.8 meV develops. The RIXS data reveals splitting of the $T_{2g}$ multiplet consistent with that seen in other $5d^3$ osmium based double perovskites. Together these results suggest that spin-orbit coupling is important for ground state selection in $3d$-$5d^3$ double perovskite materials.

DOI: 10.1103/PhysRevB.98.214422

## I. INTRODUCTION

A strong spin-orbit interaction is inherent to $4d$ and $5d$ ions, and when this is manifest in the collective properties of materials via spin-orbit coupling (SOC) it fosters a host of unconventional phases. For example, SOC is responsible for the $J_{\text{eff}} = 1/2$ electronic ground state which leads to a Mott insulating phase in $5d^5$ $Sr_2IrO_4$ [1], and Kitaev quantum-spin-liquid-like behavior in $4d^5$ $RuCl_3$ [2]. Beyond this $J_{\text{eff}} = 1/2$ paradigm, however, the influence of the spin-orbit interaction on the electronic ground state and emergent properties in $4d$ and $5d$ transition metal oxides (TMOs) has been poorly understood.

Recently, a SOC-controlled $J = 3/2$ ground state was discovered in $5d^3$ TMOs $Ba_2YOsO_6$ and $Ca_3LiOsO_6$ [3], in contrast with expectations of an orbitally quenched $S = 3/2$ singlet expected for LS coupling. Reference [3] revealed a SOC-induced splitting of the $t_{2g}^3$ manifold via resonant inelastic x-ray scattering (RIXS) measurements, which is driven by strong Os-O hybridization. This confirmed the presence of an unquenched orbital moment in the $d^3$ ion ground state, and placed these $5d^3$ materials in the intermediate coupling regime, between $LS$ and $jj$ coupling limits. There is therefore immediate interest in exploring the impact of this $J = 3/2$ ground state on the emergent properties in $d^3$ TMOs.

In the cubic double perovskite $Ba_2YOsO_6$ the direct influence of the $J = 3/2$ SOC has been observed via a spin gap in the magnetic excitation spectrum with inelastic neutron scattering [4]. More broadly, spin gaps have been observed in many single magnetic ion containing $4d^3$ and $5d^3$ double perovskites and related materials [4–9]. These results indicate that SOC directly influences the magnetic ground state in otherwise frustrated systems, which provides scope for control of the physical properties of such materials via SOC. However, for practical functional materials, the role which SOC plays in significantly noncubic materials, and in systems with more complex interactions, e.g., mixed $3d$-$5d$ systems, are open questions. Here we investigate these issues in the $3d$-$5d$ material $Sr_2FeOsO_6$.

$Sr_2FeOsO_6$ has attracted a great deal of attention due to highly tunable magnetic behavior [10–16], and because it is an unusual anomaly in the important series of compounds $Sr_2BB'O_6$, where $B$ and $B'$ are $3d$ and $4d$ or $5d$ magnetic transition metal ions, respectively. These materials are well known for their potential spintronics applications, and they generally present above room-temperature ferrimagnetism and evolve from half-metallic to insulating states as $T_C$ increases: $Sr_2FeReO_6$ $T_C = 401$ K, $Sr_2FeMoO_6$ $T_C = 420$ K, $Sr_2CrWO_6$ $T_C = 450$ K, $Sr_2CrReO_6$ $T_C = 625$ K, and $Sr_2CrOsO_6$ $T_C = 725$ K [17]. However, $Sr_2FeOsO_6$ with $Os^{5+}$ ($5d^3$, $S = \frac{3}{2}$) and $Fe^{3+}$ ($3d^5$, $S = \frac{5}{2}$) is an insulating antiferromagnet which undergoes two magnetic transitions at much lower temperatures, $T_1 = 140$ K and $T_2 = 67$ K with Fe and Os ordering in both of the magnetic phases (Fig. 1) [10].

The presence of two transitions in $Sr_2FeOsO_6$ suggests competing magnetic interactions. The competition in $Sr_2FeOsO_6$ is further demonstrated by the ease with which it can be tuned to other magnetic ground states, either by isoelectronic doping on the $A$ site [13], or via hydrostatic pressure [15], which opens a route to strain-controlled epitaxial films as functional devices [15]. Multiple first-principles calculations have attempted to identify the interactions controlling this system, yet have produced disparate results

*christiansad@ornl.gov

 

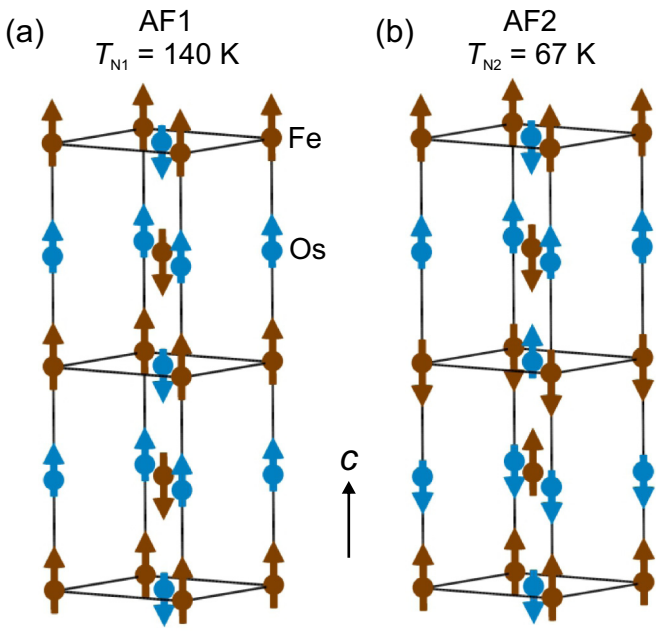


FIG. 1. Magnetic structure of $Sr_2FeOsO_6$ determined by Refs. [10,11]. (a) AF1 phase which is dominant between 140 and 67 K and (b) AF2 phase which emerges at 67 K. The Os (Fe) atoms and direction of the ordered magnetic moment are indicated by the blue (brown) circles and arrows. Two crystallographic unit cells are shown so that the changes between magnetic phases are apparent.

with predictions including semiconductor behavior [18,19], orbital order [10], dominant Fe-O-Os superexchange interactions [20], or dominant Os-O-O-Os extended superexchange [21]. None of these works considered the potential role of the recently discovered $J = 3/2$ ground state possible for the $Os^{5+}$ ions [3].

Here we experimentally probe $Sr_2FeOsO_6$ via inelastic neutron scattering (INS) and resonant inelastic x-ray scattering (RIXS). We find that despite the tetragonal distortion, SOC induced splitting of the $Os^{5+}$ $t_{2g}$ levels is observed, indicative of a $J = 3/2$ ground state. This provides a route to strong entry of SOC in this material—a factor which has not previously been explored—and this conjecture is confirmed, as we reveal a spin gap in the magnetic excitation spectrum via INS. Previously no such feature has been identified in a $3d$-$5d$ TMO, only in purely $4d$ or $5d$ materials. Unexpectedly, this SOC-induced gap only emerges below the second magnetic ordering temperature $T_2 = 67$ K. This suggests that SOC is likely intimately linked to the selection of the ground state in $Sr_2FeOsO_6$ via SOC-induced anisotropy, similar to $Ba_2YOsO_6$ and $Sr_2ScOsO_6$ [3,8]. These considerations should also apply to other $3d$-$5d^3$ combinations such as the high ordering temperature $Sr_2CrOsO_6$ [22,23].

## II. EXPERIMENTAL DETAILS

The 12.8 g polycrystalline $Sr_2FeOsO_6$ sample was synthesized by combining stoichiometric quantities of $SrO_2$, Os, $OsO_2$, and $Fe_2O_3$. Ground mixtures were contained in alumina tubes and sealed in evacuated silica vessels for heatings of 48 h at 1000 °C. This was followed by a regrinding and identical reheating. Laboratory x-ray diffraction measurements were performed to characterize the structural order of the samples studied here. Additional characterization of the structural and magnetic order was provided by neutron powder diffraction measurements performed with HB-2A at the High Flux Isotope Reactor at Oak Ridge National Laboratory (ORNL). The results of the x-ray and neutron diffraction measurements are given in the Supplemental Material [24].

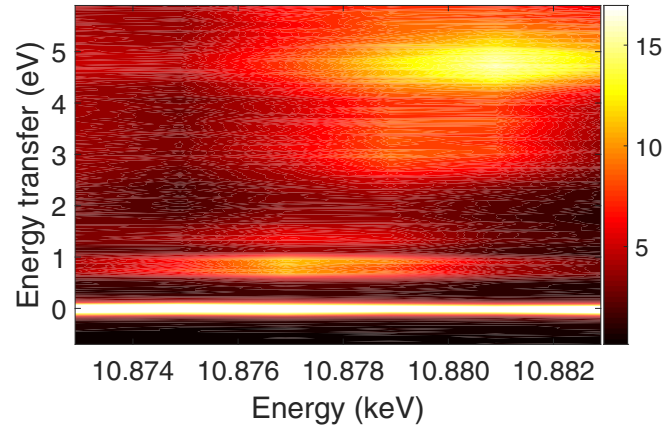


FIG. 2. RIXS data showing the incident energy dependence of electronic excitations in $Sr_2FeOsO_6$. Measurements were performed at 6 K. The color bar on the right indicates intensity in arbitrary units.

Inelastic neutron scattering measurements were performed with the SEQUOIA chopper spectrometer [25] at the Spallation Neutron Source. The sample was sealed in a flat plate Al cell with 2 mm thickness to minimize the effects of absorption. This cell and an empty cell were measured in a closed-cycle refrigerator, accessing temperatures between 5 and 170 K. Incident neutron energies ($E_i$s) of 20 and 60 meV, with Fermi chopper frequencies of 120 and 180 Hz, respectively, were used. Empty-cell background data have been subtracted from all data sets presented.

RIXS spectra were collected on a small portion of the sample on Sector 27 at the Advanced Photon Source using the MERIX instrumentation [26]. The sample temperature was controlled between 6 and 300 K in a closed-cycle refrigerator. Primary diamond(1 1 1) and secondary Si(4 0 0) monochromators were used to access the Os $L_3$ edge with a diced Si(4 6 6) analyzer yielding an energy resolution of 125 meV FWHM. Some scans were collected with a channel cut Si(4 6 6) analyzer yielding an energy resolution of 55 meV FWHM. A MYTHEN strip detector was used, and experiments were performed in horizontal geometry with $2\theta = 90°$. Data are normalized with an ion chamber monitor.

## III. RESULTS AND DISCUSSION

Figure 2 displays the excitation spectrum of $Sr_2FeOsO_6$ measured with RIXS as a function of $E_i$. As in the case of other osmium-based TMOs [3,27,28], the relative energies of the inelastic features along with the dependence of the inelastic features on $E_i$ allows for the identification of intra $t_{2g}$ processes (maximum intensity near 10.877 keV) and $t_{2g}$-$e_g$ processes (maximum intensity near 10.881 keV).

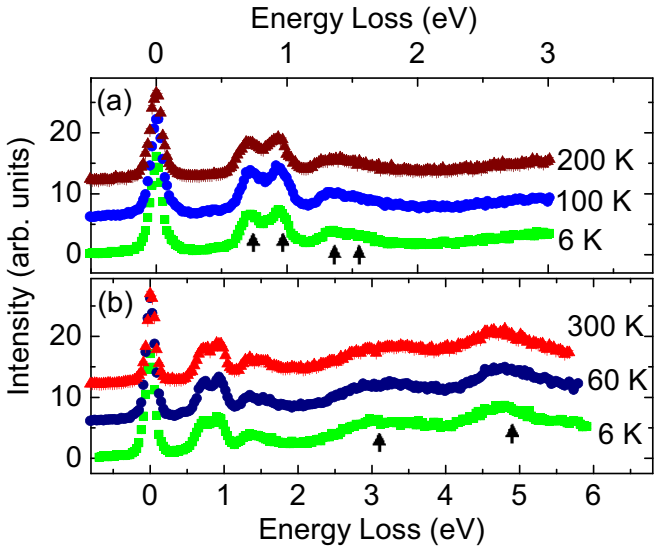


FIG. 3. RIXS data from $Sr_2FeOsO_6$. (a) High resolution data with $E_i = 10.877$ keV showing excitations (indicated by arrows) within the $t_{2g}$ multiplet. (b) Low resolution RIXS data with $E_i = 10.879$ keV. The arrows indicate the positions of excitations from the $t_{2g}$ to the $e_g$ multiplets. In (a) and (b) an offset of 6 between data sets has been added for clarity.

Figure 3 shows the RIXS spectra from $Sr_2FeOsO_6$ measured at selected temperatures in high resolution (a) and low resolution configurations (b). SOC-induced splitting of the $t_{2g}$ character excited state is apparent at all temperatures in the peaks centered around ∼0.75 eV. Peak splitting around ∼1.5 eV is not resolved, but the width which is significantly broader than instrumental resolution and the asymmetric shape of the signal indicate that two peaks are likely present, as found in $Ba_2YOsO_6$ and $Ca_3LiOsO_6$ [3]. At present it is not clear why the two peaks are not well resolved. Possibilities include the overall tetragonal symmetry and the antisite mixing with 0.856(4) Fe (Os) and 0.144(4) Os (Fe) occupancy on the $B$ ($B'$) site [24] which is within the typical range for this material [10,13,14].

The high resolution RIXS data were fit with a Gaussian peak shape, giving excited state energies of 0.723(3), 0.934(3), 1.34(1), and 1.52(2) eV at 6 K. This compares with 0.745(7), 0.971(7), 1.447(9), and 1.68(1) eV from Ref. [3] for $Ba_2YOsO_6$. As was done in Ref. [3], these data can be fit with an intermediate coupling model (under the assumption of cubic crystal field splitting) to extract values of the spin-orbit coupling $\zeta_{SOC}$ and Hund's coupling $J_h$. To prevent proliferation of fitting parameters we have fixed the Racah parameter $B$ to the value of 0.0405 eV which was determined by Ref. [29] for $5d^3$ $Re^{4+}$. Fixing $B$ to other values over a relatively broad range results in similar values of the Hunds's coupling. The model parameters are: The Racah parameters $B$ (fixed) and $C$, the crystal field splitting $10Dq$ (fixed), and the SOC $\zeta_{SOC}$. The results of the fits are insensitive to values of $10Dq$ from 3 to 4.8 eV. The resulting parameters of the fits are: $C = 0.16(1)$ eV and $\zeta_{SOC} = 0.33(5)$ eV. $J_h = 3B + C = 0.28(1)$ eV. The values are comparable to those found for $Ba_2YOsO_6$, and $Ca_3LiOsO_6$ [3], other related $5d$ containing double perovskite systems [30,31] and for $NaOsO_3$ [32,33].

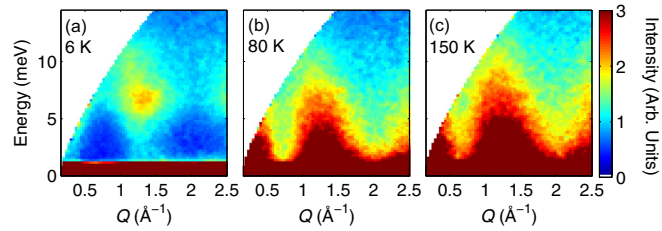


FIG. 4. Neutron scattering intensity maps with $E_i = 20$ meV showing the evolution of the scattering from (a) $T = 6$ K ($T < T_{N2}$), (b) $T = 80$ K ($T_{N2} < T < T_{N1}$), and (c) $T = 150$ K ($T > T_{N1}$). A spin gap emerges below $T_{N2}$ as seen in (a).

A distinction between the RIXS data for $Sr_2FeOsO_6$ and other $5d^3$ systems is that there appears to be two excitations between the $t_{2g}$ and the $e_g$ multiplets. These are found to be at 3.05(3) and 4.85(6) eV [indicated by arrows in Fig. 3(b)]. At the present time we do not have an explanation for this observation and so discuss some possibilities in the remainder of the paragraph. The overall tetragonal symmetry of $Sr_2FeOsO_6$ is likely not the reason for the appearance of the two features. At the lowest temperatures the oxygen octahedra surrounding the osmium ions are nearly cubic [13,14] and both features are observed in the RIXS spectra at all temperatures measured with minimal variation. Another possibility is that the antisite mixing between Fe and Os provides two environments for Os resulting in the two peak structure. We speculate that another possibility is that the Hund's coupling on Fe and strong Os-O and O-Fe hybridization for an $e_g$ orbital results in a large splitting for spin flip and spin parallel excitations from the $t_{2g}$ to the $e_g$ on Os. Confirmation of this idea is left as the subject of future work.

An overview of the measured INS spectra from 6, 80, and 150 K is shown in Fig. 4. While there is no significant change in the inelastic spectrum upon crossing $T_{N1}$, below $T_{N2}$ there is a pronounced change in the excitation spectrum, as a gap opens and the intensity is concentrated at higher energies, see 6 K data. This behavior is reminiscent of the observed gap development below $T_N$ in the previously measured single-magnetic-ion $4d^3$ and $5d^3$ double perovskites [4–6,8] and indicates the development of SOC induced anisotropy below $T_{N2}$ in $Sr_2FeOsO_6$. Note that at the lowest temperatures where the spin gap is the strongest, the octahedra surrounding Os are more symmetric [13,14] than at higher temperatures indicating that a structural distortion at $T_{N2}$ is not likely the origin of the observed gap.

The detailed $(Q, E)$-space temperature dependence of the scattering is presented in Fig. 5. Constant-energy cuts averaged over $2 < E < 3$ meV, i.e., within the gap, are shown in Fig. 5(a). Intensity is observed around wave vector $Q \approx 0.4$ Å$^{-1}$, which we attribute to scattering near the magnetic wave vector $Q_{AF2} = |(0\,0\,\frac{1}{2})| = 0.39$ Å$^{-1}$. $Q_{AF2} = (0\,0\,\frac{1}{2})$ is not an observed magnetic Bragg reflection because the magnetic moments lie along the $c$ axis and only moments perpendicular to $Q$ give neutron scattering intensity. Transverse magnetic fluctuations emerging from $(0\,0\,\frac{1}{2})$, however, have a moment perpendicular to $Q$ and can therefore be observed, as in Figs. 4 and 5(a). Therefore the scattering at this purely AF2 wave vector are associated with interactions responsible for the AF2 magnetic order. The $Q \approx 1.3$ Å$^{-1}$ centered signal in

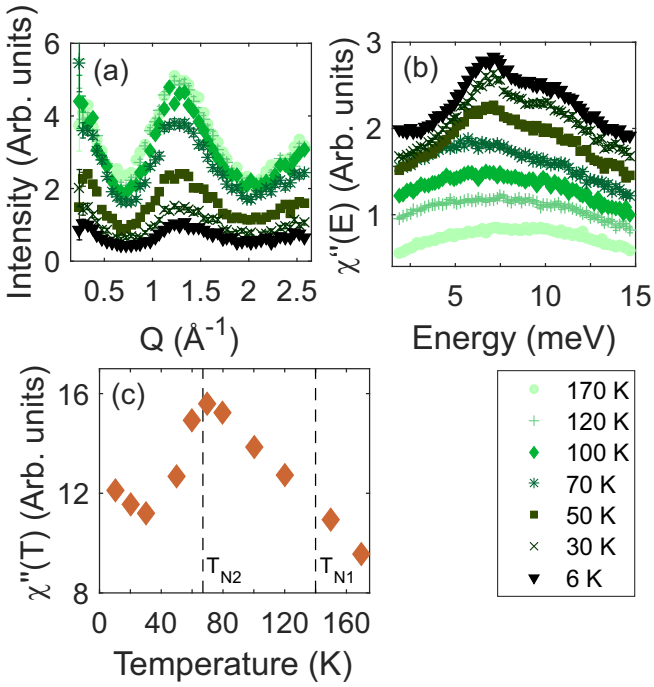


FIG. 5. (a) Measured intensity of neutron scattering data averaged over 2–3 meV at temperatures as indicated in the legend in the lower right. (b) Constant-wave vector cuts averaged over 0.8–1.8 Å$^{-1}$ which have been corrected for the Bose population factor $1/[1-\exp(-E/k_BT)]$. Successive cuts have been offset by 0.2. (c) Data averaged over 2–3 meV and 0.8–1.8 Å$^{-1}$ and corrected for the Bose factor as a function of temperature, demonstrating temperature dependence of the scattering within the gap. All panels show data collected with $E_i = 20$ meV. In (b) and (c) the error bars are smaller than the symbols.

Figs. 4 and 5(a) is a combination of scattering from $Q_{AF1} = (1\,0\,0)$, and $Q_{AF2} = (0\,0\,\frac{3}{2})$ and $(1\,0\,\frac{1}{2})$ magnetic wave vectors, which cannot be resolved in this measurement. Inspecting Fig. 5(a) it is clear that the fluctuations do not go to zero within the gap at 6 K, which is the result of the presence of a significant fraction (31%) of gapless phase 1 remaining at this temperature (see Fig. S2 and associated discussion [24] and Refs. [10,11]).

To track the relative strength of the fluctuations with temperature, the data in Figs. 5(b) and 5(c) have been corrected for the Bose thermal population factor, giving the results in terms of the dynamic susceptibility $\chi''(Q, E)$. The constant-wave vector cuts, averaged over 0.8–1.8 Å$^{-1}$, in Fig. 5(b) show that there is a significant build up of spectral weight in the range ~5–13 meV below $T_{N2}$. There is little change in the energy dependence of the scattering at the first transition, $T_{N1} = 140$ K. The onset of the gapped magnetic scattering intensity at low temperature appears to be at $E \approx 5$ meV, and the peak of the intensity is at 6.8(1) meV, determined by fitting two Gaussians on a flat background to the 6 K cut shown in Fig. 5(b). The second peak in intensity is determined to be 10.5(1) meV. The observation of two peaks within the band is consistent with the effects of powder averaging the magnetic excitation signals originating from the inequivalent directions present in the tetragonal crystal structure, as seen in other significantly distorted double perovskites [6]. We compare the peak of the lower band $\Delta = 6.8(1)$ meV to previous observations of the gap in $4d^3$ and $5d^3$ double perovskites, as these have followed the convention of using the center of the acoustic band as an estimate of the value of the gap. In $Sr_2ScOsO_6$, $Ba_2YOsO_6$, $Ba_2YRuO_6$, and $La_2NaRuO_6$ the determined values are $\Delta = 19(2)$ meV, $\Delta = 18(2)$ meV, $\Delta \approx 5$ meV, and $\Delta \approx 2.75$ meV, respectively [4–6]. Notably, the energy scale of the gap in $Sr_2FeOsO_6$ is significantly lower than $Os^{5+}$ counterparts $Sr_2ScOsO_6$ and $Ba_2YOsO_6$, but still larger than the $Ru^{5+}$ examples, in which spin-orbit effects are expected to be reduced. We note that attempts were made to extract the exchange interactions from spin-wave models of the INS spectra, however the multiple magnetic ions and associated exchange paths result in too many fitting parameters to be properly constrained by the powder averaged inelastic neutron scattering data reported here.

Another method of estimating the gap was used by Kermarrec *et al.* [4] for $Ba_2YOsO_6$, in which $\chi''(T)$ for $E < \Delta$ is compared to that expected for a thermally activated excitation, i.e., $\chi''(T < T_{N2}) \propto \exp(-\Delta/k_BT)$. While we see a drop in $\chi''(T)$ below $T_{N2}$ in Fig. 5, instead of a plateau above $T_{N2}$, as in $Ba_2YOsO_6$, the intensity steadily increases with decreasing temperature towards a maximum at $T_{N2}$. We attribute the steady increase predominantly to the competition between phase 1 and phase 2. Similarly, at very low temperatures $\chi''(T)$ shows a slight upturn, which we attribute to the remaining ungapped AF1 fraction increasingly tending towards AF2 order. Therefore, the temperature dependence in the region $T < T_{N2}$ is not expected to follow a $\exp(-\Delta/k_BT)$ dependence, but instead is a combination of this reduction in intensity with the steadily increasing intensity due to the tendency of the AF1 fraction towards AF2.

## IV. CONCLUSIONS

The measurements presented have demonstrated that a SOC-induced gap does emerge in the $3d$-$5d^3$ system $Sr_2FeOsO_6$, but only below the second magnetic transition temperature. The neutron diffraction results show that at all temperatures the AF1 and AF2 magnetic phases are associated with different structural phases [24]. These observations together confirm the notion that the lattice, magnetic, and orbital degrees of freedom in this material are all intimately linked. It is worth pointing out that the mixing of Fe and Os sites in this material might be taken to suggest that there are two phases associated with separated Fe-rich and Os-rich regions. However, the constant evolution of the AF1 to AF2 phases below 67 K establishes that there is real competition between these phases not associated with stoichiometry (although local stoichiometry may influence $T_{N2}$). $^{57}$Fe Mössbauer spectroscopy supports this interpretation [11]. Therefore, it appears that SOC is an essential component in selection of the magnetic ground states in $Sr_2FeOsO_6$ as was found for $Sr_2ScOsO_6$ [8] suggesting that similar considerations are important for understanding the ground states and high ordering temperatures in other $3d$-$5d^3$ TMOs.

The Department of Energy will provide public access to these results of federally sponsored research in accordance with the DOE Public Access Plan [34].

## ACKNOWLEDGMENTS

This work was supported by the U.S. Department of Energy, Office of Science, Basic Energy Sciences, Materials Sciences and Engineering Division. The research at ORNL's Spallation Neutron Source and High Flux Isotope Reactor was supported by the Scientific User Facilities Division, Office of Basic Energy Sciences, U.S. Department of Energy (DOE). Use of the Advanced Photon Source at Argonne National Laboratory was supported by the U.S. Department of Energy, Office of Science, Office of Basic Energy Sciences, under Contract No. DE-AC02-06CH11357. This research was supported in part by the Center for Emergent Materials a National Science Foundation (NSF) Materials Research Science and Engineering Center (DMR-1420451). R.M. acknowledges support from the Alexander von Humboldt Foundation. A.P. acknowledges funding from NSERC of Canada.

This manuscript has been authored by employees of UT-Battelle, LLC under Contract No. DE-AC05-00OR22725 with the U.S. Department of Energy. The U.S. Government retains and the publisher, by accepting the article for publication, acknowledges that the U.S. Government retains a nonexclusive, paid-up, irrevocable, worldwide license to publish or reproduce the published form of this manuscript or allow others to do so for U.S. Government purposes.



[1] B. J. Kim, H. Ohsumi, T. Komesu, S. Sakai, T. Morita, H. Takagi, and T. Arima, Science **323**, 1329 (2009).

[2] A. Banerjee, C. A. Bridges, J.-Q. Yan, A. A. Aczel, L. Li, M. B. Stone, G. E. Granroth, M. D. Lumsden, Y. Yiu, J. Knolle, S. Bhattacharjee, D. L. Kovrizhin, R. Moessner, D. A. Tennant, D. G. Mandrus, and S. E. Nagler, Nat. Mater. **15**, 733 (2016).

[3] A. E. Taylor, S. Calder, R. Morrow, H. L. Feng, M. H. Upton, M. D. Lumsden, K. Yamaura, P. M. Woodward, and A. D. Christianson, Phys. Rev. Lett. **118**, 207202 (2017).

[4] E. Kermarrec, C. A. Marjerrison, C. M. Thompson, D. D. Maharaj, K. Levin, S. Kroeker, G. E. Granroth, R. Flacau, Z. Yamani, J. E. Greedan, and B. D. Gaulin, Phys. Rev. B **91**, 075133 (2015).

[5] J. P. Carlo, J. P. Clancy, K. Fritsch, C. A. Marjerrison, G. E. Granroth, J. E. Greedan, H. A. Dabkowska, and B. D. Gaulin, Phys. Rev. B **88**, 024418 (2013).

[6] A. A. Aczel, P. J. Baker, D. E. Bugaris, J. Yeon, H.-C. zur Loye, T. Guidi, and D. T. Adroja, Phys. Rev. Lett. **112**, 117603 (2014).

[7] S. M. Disseler, J. W. Lynn, R. F. Jardim, M. S. Torikachvili, and E. Granado, Phys. Rev. B **93**, 140407(R) (2016).

[8] A. E. Taylor, R. Morrow, R. S. Fishman, S. Calder, A. I. Kolesnikov, M. D. Lumsden, P. M. Woodward, and A. D. Christianson, Phys. Rev. B **93**, 220408(R) (2016).

[9] S. Calder, D. J. Singh, V. O. Garlea, M. D. Lumsden, Y. G. Shi, K. Yamaura, and A. D. Christianson, Phys. Rev. B **96**, 184426 (2017).

[10] A. K. Paul, M. Reehuis, V. Ksenofontov, B. Yan, A. Hoser, D. M. Többens, P. M. Abdala, P. Adler, M. Jansen, and C. Felser, Phys. Rev. Lett. **111**, 167205 (2013).

[11] P. Adler, V. Ksenofontov, A. K. Paul, M. Reehuis, B. Yan, M. Jansen, and C. Felser, Hyperfine Interact. **226**, 289 (2013).

[12] H. L. Feng, M. Arai, Y. Matsushita, Y. Tsujimoto, Y. Guo, C. I. Sathish, X. Wang, Y.-H. Yuan, M. Tanaka, and K. Yamaura, J. Am. Chem. Soc. **136**, 3326 (2014).

[13] R. Morrow, J. W. Freeland, and P. M. Woodward, Inorg. Chem. **53**, 7983 (2014).

[14] A. K. Paul, M. Jansen, B. Yan, C. Felser, M. Reehuis, and P. M. Abdala, Inorg. Chem. **52**, 6713 (2013).

[15] L. S. I. Veiga, G. Fabbris, M. van Veenendaal, N. M. Souza-Neto, H. L. Feng, K. Yamaura, and D. Haskel, Phys. Rev. B **91**, 235135 (2015).

[16] R. C. Williams, F. Xiao, I. O. Thomas, S. J. Clark, T. Lancaster, G. A. Cornish, S. J. Blundell, W. Hayes, A. K. Paul, C. Felser, and M. Jansen, J. Phys.: Condens. Matter **28**, 076001 (2016).

[17] S. Vasala and M. Karppinen, Prog. Solid State Chem. **43**, 1 (2015).

[18] J. Wang, J. Meng, and Z. Wu, Chem. Phys. Lett. **501**, 324 (2011).

[19] J. Wang, N. Zu, X. Hao, Y. Xu, Z. Li, Z. Wu, and F. Gao, Phys. Status Solidi RRL **08**, 776 (2014).

[20] Y. S. Hou, H. J. Xiang, and X. G. Gong, Sci. Rep. **5**, 13159 (2015).

[21] S. Kanungo, B. Yan, M. Jansen, and C. Felser, Phys. Rev. B **89**, 214414 (2014).

[22] Y. Krockenberger, K. Mogare, M. Reehuis, M. Tovar, M. Jansen, G. Vaitheeswaran, V. Kanchana, F. Bultmark, A. Delin, F. Wilhelm, A. Rogalev, A. Winkler, and L. Alff, Phys. Rev. B **75**, 020404(R) (2007).

[23] R. Morrow, J. R. Soliz, A. J. Hauser, J. C. Gallagher, M. A. Susner, M. D. Sumption, A. A. Aczel, J. Yan, F. Yang, and P. M. Woodward, J. Solid State Chem. **238**, 46 (2016).

[24] See Supplemental Material at http://link.aps.org/supplemental/10.1103/PhysRevB.98.214422 where we discuss additional details regarding the sample characterization.

[25] M. B. Stone, J. L. Niedziela, D. L. Abernathy, L. DeBeer-Schmitt, G. Ehlers, O. Garlea, G. E. Granroth, M. Graves-Brook, A. I. Kolesnikov, A. Podlesnyak, and B. Winn, Rev. Sci. Instrum. **85**, 045113 (2014).

[26] T. Gog, G. T. Seidler, D. M. Casa, M. H. Upton, J. Kim, S. Stoupin, K. P. Nagle, M. Balasubramanian, R. A. Gordon, T. T. Fister, S. M. Heald, T. Toellner, J. P. Hill, D. S. Coburn, Y.-J. Kim, A. H. Said, E. E. Alp, W. Sturhahn, H. Yavas, C. A. Burns, and H. Sinn, Synchrotron Rad. News **22**, 12 (2009).

[27] S. Calder, J. G. Vale, N. A. Bogdanov, X. Liu, C. Donnerer, M. H. Upton, D. Casa, A. H. Said, M. D. Lumsden, Z. Zhao, J.-Q. Yan, D. Mandrus, S. Nishimoto, J. van den Brink, J. P. Hill, D. F. McMorrow, and A. D. Christianson, Nat. Commun. **7**, 11651 (2016).

[28] S. Calder, J. G. Vale, N. Bogdanov, C. Donnerer, D. Pincini, M. Moretti Sala, X. Liu, M. H. Upton, D. Casa, Y. G. Shi, Y. Tsujimoto, K. Yamaura, J. P. Hill, J. van den Brink, D. F. McMorrow, and A. D. Christianson, Phys. Rev. B **95**, 020413(R) (2017).

[29] P. B. Dorain and R. G. Wheeler, J. Chem. Phys. **45**, 1172 (1966).

[30] B. Yuan, J. P. Clancy, A. M. Cook, C. M. Thompson, J. Greedan, G. Cao, B. C. Jeon, T. W. Noh, M. H. Upton, D. Casa,

T. Gog, A. Paramekanti, and Y.-J. Kim, Phys. Rev. B **95**, 235114 (2017).

[31] A. Paramekanti, D. J. Singh, B. Yuan, D. Casa, A. Said, Y.-J. Kim, and A. D. Christianson, Phys. Rev. B **97**, 235119 (2018).

[32] J. G. Vale, S. Calder, C. Donnerer, D. Pincini, Y. G. Shi, Y. Tsujimoto, K. Yamaura, M. M. Sala, J. van den Brink, A. D. Christianson, and D. F. McMorrow, Phys. Rev. Lett. **120**, 227203 (2018).

[33] J. G. Vale, S. Calder, C. Donnerer, D. Pincini, Y. G. Shi, Y. Tsujimoto, K. Yamaura, M. Moretti Sala, J. van den Brink, A. D. Christianson, and D. F. McMorrow, Phys. Rev. B **97**, 184429 (2018).

[34] http://energy.gov/downloads/doe-public-access-plan.